We are IntechOpen, the world's leading publisher of Open Access books Built by scientists, for scientists

6,900
Open access books available

185,000
International authors and editors

200M
Downloads

Our authors are among the

154
Countries delivered to

TOP 1%
most cited scientists

12.2%
Contributors from top 500 universities

CLARIVATE ANALYTICS
BOOK CITATION INDEX
INDEXED

WEB OF SCIENCE™

Selection of our books indexed in the Book Citation Index
in Web of Science™ Core Collection (BKCI)

Interested in publishing with us?
Contact book.department@intechopen.com

Heterodyne Interferometer for Measurement of Electron Density in High-Pressure Plasmas

Keiichiro Urabe and Kunihide Tachibana
Kyoto University
Japan

1. Introduction

Conventional material processes using plasmas generated in low pressure gaseous media are recently being transposed to high-pressure plasma processes, because of the potential of high-pressure plasmas to reduce costs for vacuum systems in industrial applications. In many kinds of high-pressure plasma sources, small-scale atmospheric-pressure plasmas (APPs) having a property of thermal non-equilibrium, have been especially attracting much interest of researchers over the last 20 years (Becker, 2005). In such a high pressure gaseous medium, generating the small-scale plasmas in mm or μm order is effective to keep its ignition voltage low and discharge behavior stable, following a famous rule on discharge ignition called a "Paschen's law" (Paschen, 1889; von Engel, 1994). Using these small-scale high-pressure plasmas, localized maskless processes, for example etching (Ichiki et al., 2004) and deposition (Babayan et al., 1998), have been reported. Also, nanomaterial synthesis was realized by the APP utilizing their property of short residence time of source particles inside the plasma (Nozaki et al., 2007). In addition to the inorganic solid material processes, process objects of the APPs are spreading toward liquids (Bruggeman & Leys, 2009) and biocells (Kong et al., 2009) which cannot present in low-pressure conditions.

In characterization and comparison of plasma properties, electron density is one of the most important parameters. This is because that electrons play a major role for carrying external energy to heavy particles inside the plasma, and all other excited species can be calculated theoretically from the plasma parameters of electron density, electron energy distribution, and gas composition. Diagnostics of electron density have in the APPs have been reported by many researchers using Langmuir probe methods (Chang, 1973; Chang & Laframboise, 1976), Stark broadening measurement (Laux et al., 2003), and laser Thomson scattering measurement (Kono & Iwamoto, 2004). However, these methods have limitations for the APP measurements due to their finite sensitivies, expected perturbations or interferences, spatiotemporal resolutions, etc. For instance, the Langmuir probe is difficult be applied to the small-scale APPs since its theory in a collision dominant condition is not well developed and there are discharge perturbations by the metallic probe. The Stark broadening spectroscopic method enables us to derive electron density only for over 5×10^{13} cm^{-3} due to the large pressure broadening superposed over the Lorentzian shape (Laux et al., 2003). The laser Thomson scattering method is not applicable to molecular gases although its spatial resolution is high enough, because large Raman scattering components overlap with the Thomson scattering signal.

For the purpose of diagnostics in the small-scale high-pressure plasmas, refractive-index measurement using electromagnetic (EM) waves is appropriate since they can provide plasma property's information with negligible perturbation to the plasma. Also, in the refractive-index measurement, we can ignore excitation and scattering processes that are largely dependent on gas compositions and densities, which are indispensable for the above listed other measurement methods. For typical APPs whose electron densities range from 10^{12} to 10^{15} cm^{-3}, microwaves and millimeter-waves are suitable to detect absorption of the probing EM waves and derive the electron density from the absorption ratio (Tachibana et al., 2005(a), 2005(b); Sakai et al., 2005; Ito et al., 2010). However, diagnostics using those EM waves cannot have good spatial resolutions for the small-scale plasmas because of their diffraction limits. Meanwhile, a heterodyne interferometer of CO₂ laser beam, which is a theme in this chapter, can be in a category of the refractive-index measurement methods and have a good spatial resolution at the same time. This interferometer detects the laser beam's phase shift caused by the presence of tested plasma and provides line-integrated information of electron density with a spatial resolution in sub mm order (Leipold et al., 2000; Choi et al., 2009).

This chapter is focused on descriptions of the CO₂-laser heterodyne interferometer for the measurement in small-scale high-pressure plasma sources, because detailed descriptions of the interferometer for the low-pressure plasmas have been written in other chapters and textbooks (*for example* Hutchinson, 2002). In high-pressure plasmas, large contribution of gas-particle density (atoms and/or molecules in ground states) to the change of the refractive index is expected due to Joule heating in the discharge region, and this must be accurately separated from the signal in order to derive the absolute value of electron density. Therefore, we firstly explain how to divide the two components in the CO₂-laser beam's phase shift, which are the phase shifts due to electron generation and gas heating. Then, the fundamental properties of our CO₂-laser heterodyne interferometer, for example spatial resolution and lower limit of electron-density detection, are verified reviewing experimental measurements of the small-scale APPs driven by DC applied voltages (Choi et al., 2009). Finally, a combination measurement method composed of the CO₂-laser heterodyne interferometer and a millimeter-wave transmission method is introduced as a solution of spatiotemporally resolved electron-density measurement in small-scale APPs with high-speed temporal evolution of electron density (Urabe et al., 2011).

2. Fundamentals of heterodyne interferometer

This section includes brief introduction of a Mach-Zehnder principle and a heterodyne technique used in our interferometer and theoretical descriptions of the phase shift in the CO₂ laser beam induced by electrons in a tested plasma source, and explanations how to derive electron density in small-scale high-pressure plasmas eliminating influence of gas heating from total phase shift signals.

2.1 Mach-Zehnder heterodyne interferometer

Measurements of refractive index in tested materials are often done by some forms of interferometer. Most of interferometers are in Michelson, Fabry-Perot, and Mach-Zehnder configurations. Mach-Zehnder interferometer is a two-beam interferometer having two paths in which the laser beams travel in only one direction. The original laser beam is

separated by a beam splitter, and the beam's phase change is caused by variations of the refractive index of the tested material placed only in one path. Difference of the refractive indexes between the two paths is derived from the merged beam by a second beam splitter.

A heterodyne technique is a reducing method of observing frequency from light frequency to external oscillator frequency in a instrumentally manageable range. When this method is applied to the Mach-Zehnder interferometer, the light frequency in one of two paths is modulated, and in the other path the frequency is not modulated but its phase is shifted by the tested material. After merging the two laser beams, a beat signal at the modulation frequency in the merged beam can be isolated from the original output signal of a solid-state detecting device, $I(t)$, which is expressed in a following equation.

$$I(t) = \left| U_1(t) + U_2(t) \right|^2_{\omega=0} = E_1^2 + E_2^2 + E_1 E_2 \cos(\Delta\omega t - \Delta\Phi), \tag{1}$$

where $U_1(t) = E_1\cos(\omega t + \Delta\omega t)$ is the electric field of the laser beam passing through the frequency modulating device with a modulation frequency at $\Delta\omega$, $U_2(t) = E_2\cos(\omega t + \Delta\Phi)$ is the electric field of the beam passing through the tested material, and $\Delta\Phi$ is the phase shift of the beam by the tested material. Components in a light frequency range are automatically eliminated from the signal because of the response-speed limitation of detectors. From the output signal, $I(t)$, we can derive the phase shift by the tested material $\Delta\Phi$ using a phase detecting device and a reference signal which is separated from the frequency-modulation signal.
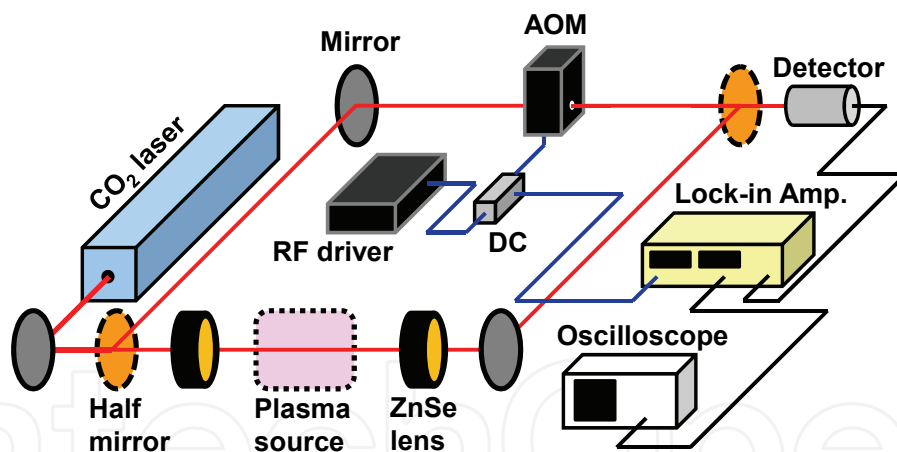

Fig. 1. Experimental setup of CO_2-laser heterodyne interferometer in Mach-Zhender principle for measurement of electron density inside high-pressure plasma source. AOM is acousto optical modulator shifting CO_2-laser frequency at frequency of RF driver's signal. DC is directional coupler taking small amplitude of RF signal driving AOM to input reference signal to lock-in amplifier.

A practical experimental setup of the CO_2-laser heterodyne interferometer used in our studies is shown in Fig. 1. The original CO_2 laser beam was split by a ZnSe half mirror. The beam frequency in one path was shifted an acousto-optical modulator (AOM) whose modulation frequency $\Delta\omega$ = 40 MHz. In the other path, the beam was focused on a tested plasma source by a pair of ZnSe lens, and the beam phase was shifted by the tested plasma. These two beams were superposed again at another ZnSe half mirror, and their beat signal

was detected by a HgCdTe IR detector operated at room temperature. The output signal of the IR detector, $I(t)$, was put into a lock-in amplifier with the reference signal, $\cos(\Delta\omega t)$, which was divided from a RF signal driving the AOM by a directional coupler (DC). The lock-in amplifier outputs a signal proportional to the phase shift, $\Delta\Phi$, and its temporal evolution was recorded in an oscilloscope.

2.2 Phase shift of CO₂ laser beam by electrons inside plasmas

In refractive-index measurement inside a tested plasma source having no gas temperature fluctuation, for example plasmas generated in gaseous media at very lower pressure than atmosphere, the phase shift by tested plasma, $\Delta\Phi$, measured using the Mach-Zehnder heterodyne interferometer becomes

$$\Delta\Phi = \int (k_{\text{plasma}} - k_0)\, dl = \int (N_{\text{plasma}} - 1)\frac{2\pi}{\lambda}\, dl \,, \tag{2}$$

where k_{plasma} and k_0 are the wavenumbers of the plasma and vacuum, N_{plasma} is the refractive index of the plasma, and λ is the wavelength of the CO₂ laser beam. Absolute electron density inside the plasma, n_e (m), can be derived using a following relationship.

$$N_{\text{plasma}} = \sqrt{1 - \omega_{\text{plasma}}^2 \Big/ \omega^2} \approx 1 - \frac{1}{2}\left(\omega_{\text{plasma}}^2 \Big/ \omega^2\right) = 1 - \frac{1}{2}\frac{n_e e^2}{m_e \varepsilon_0}\frac{\lambda^2}{4\pi^2 c^2} \,, \tag{3}$$

where ω_{plasma} and ω are the electron plasma frequency and the angular frequency of laser beam, m_e is the mass of electron, ε_0 is the permittivity of vacuum, c is the velocity of light (Hutchinson, 2002). We used an approximate expansion in this calculation because electron density is sufficiently smaller than gas-particle density in weakly ionized plasmas generated in laboratories. When we assume that electron density inside the tested plasma is spacially homogeneous and its length along the laser path is d (m), the relationship between the phase shift and the electron density becomes

$$\Delta\Phi = (N_{\text{plasma}} - 1)\frac{2\pi}{\lambda}d = -\frac{e^2\lambda}{4m_e\varepsilon_0\pi c^2}n_e d \approx -\left(3.0\times10^{-20}\right)n_e d \ \ (\text{rad}), \tag{4}$$

in the CO₂-laser heterodyne interferometer at $\lambda = 10.6$ μm.

2.3 Electron-density measurement in high-pressure plasmas

In this subsection, influence of dense gas particles in high-pressure plasmas on the calculation of electron density from the phase shift of the CO₂ laser beam, which can be ignored in the measurement of low-pressure plasmas, is introduced. It should be noted that increase of gas temperature corresponding to decrease of gas-particle density is promoted in the high-pressure plasmas because of high collision frequencies between electrons and gas particles. This change of gas-particle density results in the change of the refractive index in gaseous medium. The refractive index of the gaseous medium, N_{gas}, is

$$N_{\text{gas}} = 1 + A\left(1 + \frac{B}{\lambda^2}\right)\frac{n_g}{n_{g0}} \,, \tag{5}$$

where A and B are the specific values for gas species, n_{g0} is the gas particle density under the standard temperature and pressure (STP) conditions, and n_g is the gas-particle density inside the tested plasma source (Allen, 1973). Considering the influence of gas-particle density on the refractive index, the phase shift of the CO_2 laser beam in the high-pressure plasmas is described by two components of the electron density, $\Delta\Phi_e$, and the gas-particle density, $\Delta\Phi_g$, as a following equation.

$$\Delta\Phi = \Delta\Phi_e + \Delta\Phi_g = -\frac{e^2\lambda}{4m_e\varepsilon_0\pi c^2}n_e d + \frac{2\pi A}{\lambda n_{g0}}\left(1 + \frac{B}{\lambda^2}\right)n_g d. \qquad (6)$$

Table 1 lists change directions of the phase shift in the CO_2-laser heterodyne interferometer. Whereas we used the gas-particle density n_g for the calculation in Eq. (6), $\Delta\Phi_g$ can be also expressed using gas temperature in the plasma. Each component of the phase shift in the high-pressure plasma, $\Delta\Phi_e$ and $\Delta\Phi_g$, changes to negative direction due to the electron production and the decrease of gas-particle density by the Joule heating. The separation of these two components becomes a crucial problem for accurate derivation of the electron density in practical measurements of the high-pressure plasmas, because these two components are only measured together in the heterodyne interferometer and start decreasing at the same timing.

	Increase	Decrease
Electron density	Negative	Positive
Gas-particle density	Positive	Negative
Gas temperature	Negative	Positive

Table 1. Change directions of CO_2-laser beam's phase shift by changes of electron density, gas-particle density, and gas temperature, when they increase or decrease.

For the separation of two components in the phase shift of the CO_2 laser beam, difference of time constants of the two phenomena is utilized, because the change of electron density is much faster than that of gas temperature in the high-pressure discharge (Leipold et al., 2000; Choi et al., 2009). Applicability of this technique can be confirmed by experimental evidence as explained below. Also, in general, the two terms of electron density, n_e, and gas-particle density, n_g, can be derived directly by solving a system of two equations using a two-wavelength heterodyne interferometer, because the phase-shift components due to the electron and gas-particle densities depend differently on the laser wavelength. Some groups have tried to measure both electron and gas-particle densities inside the plasma by an additional heterodyne interferometer using a He-Ne laser beam at 633 nm (Adler & Kindel, 2003; Acedo et al., 2004).

Figure 2 shows an example waveform of the output phase-shift signal of the lock-in amplifier obtained in a small-scale high-pressure plasma source operated at 70 Torr driven by a pulsed DC voltage at 300 V with a 300-μs pulse duration. The phase-shift signal recorded in the oscilloscope is proportional to the phase shift in a specification ratio of the

lock-in amplifier. Around 50 µs after the discharge ignition, the phase shift decreased rapidly in 150 µs, and then a slower change followed until the discharge termination. The 50-µs delay of the phase-shift signal is due to calculating delay time of the phase shift in the lock-in amplifier. The initial faster falling part is attributed to the increase of electron density, and the second slower part is to the decrease of gas-particle density by the Joule heating. Faster and slower slopes of the phase shift similar to the ignition timing were also observed in the termination timing. Subtracting the phase-shift component of gas-particle density, $\Delta\Phi_g$, shown in a blue dashed-dotted curve in Fig. 2, the component of electron density, $\Delta\Phi_e$, was obtained as shown in a red dashed curve. The absolute value of electron density can be derived from the amplitude of electron-density component.
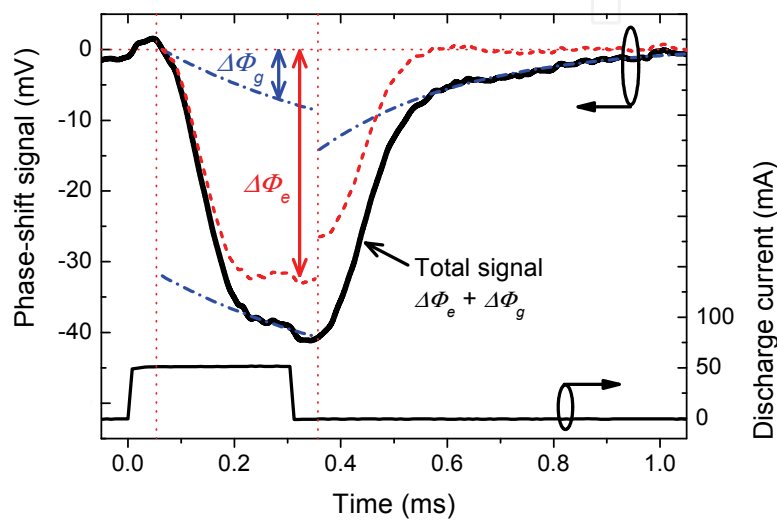
Fig. 2. Temporal evolutions of phase-shift signal from lock-in amplifier and discharge current. Tested plasma source is small-scale discharge driven by 300-V pulsed DC high voltage at 70 Torr of He gas (Choi et al., 2009).
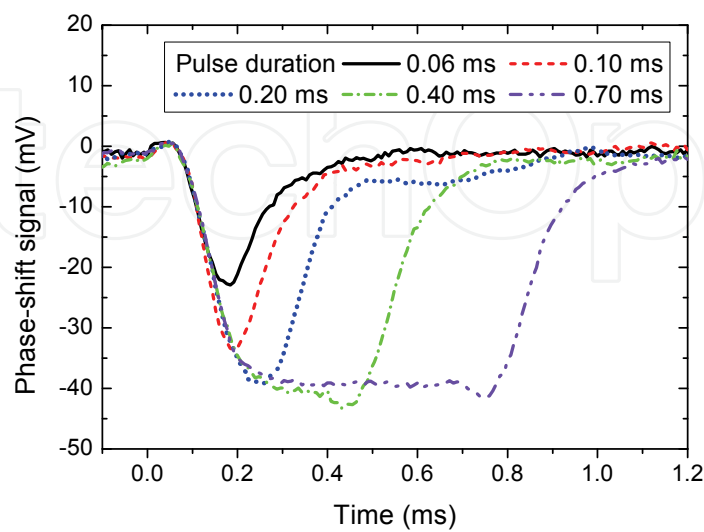

Fig. 3. Temporal evolutions of phase-shift signal measured changing voltage pulse duration from 60 to 700 µs (Choi et al., 2009).

As explained in the previous paragraph, because the temporal changes of electron and gas-particle density can be observed only in the discharge ignition or termination timings, there is a need to pulse modulation of continuous discharge for the separation of phase-shift components measured in the CO_2-laser heterodyne interferometer. In order to understand appropriate range of duration times for the pulse modulation, especially minimum duration time, it is important to measure the phase-shift signal decreasing the modulating pulse duration. Figure 3 shows waveforms of the phase-shift signal measured in our heterodyne interferometer using five pulse duration times ranging from 60 to 700 μs. From the measured waveforms, it could be confirmed that the pulse modulation with the duration time shorter than 200 μs does not give us accurate information of electron density in our setup, and we used the modulation pulse with duration times larger than 500 μs in our studies. This temporal behavior of the output signal of the heterodyne interferometer is of course different in each IR detector and phase measuring system.
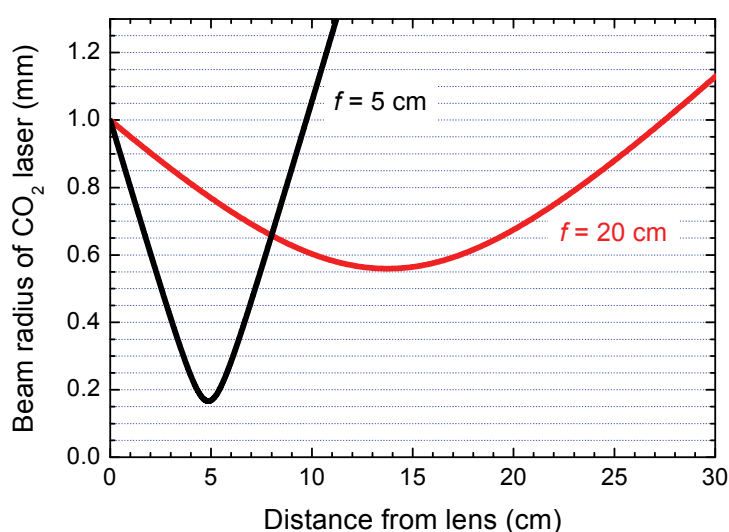

Fig. 4. Calculated beam spot radii of CO_2 laser beam at 10.6 μm as a function of distance from lens (Yariv, 1997). Initial spot radius at 1.0 mm and focal lengths of lens at 5 and 20 cm correspond to practical conditions used in our experiments.

For measuring the spatial distributions of electron density, evaluation of the spot radius of the CO_2 laser beam inside the tested plasma source is required. In order to measure the spatial distribution of electron density inside the high-pressure plasmas whose scale are usually below cm order, the CO_2-laser beam has to be focused in μm order using a pair of ZnSe lens as shown in Fig. 1. Assuming that the laser beam is a Gaussian beam, we can calculate a profile of the beam spot radius along the laser path from the beam parameter and focal length of the ZnSe lens using an ABCD matrix analysis (Yariv, 1997). Figrue 4 shows the beam-radius profiles after the two kinds of ZnSe lens used in our experimental study. The location and length of the tested plasma source and a scanning pitch of the laser beam should be determined by reference to these kinds of beam-profile evaluations.

3. Spatial distribution of electron density in high-pressure plasmas

Some of the specific measurement results of our CO_2-laser heterodyne interferometer are introduced in this section. Influence of gas heating on detected phase-shift signals, spatial

resolutions of the heterodyne interferometer, and the combination measurement method for AC-voltage driven APPs, will be discussed in addition to the measured electron-density distributions in the tested plasma sources.

3.1 Small-scale DC discharge at high pressure

A short hollow cathode (HC) discharge tube shown in Fig. 5(a) was used for basic experiments of our CO_2-laser heterodyne interferometer system with variable pressure in pure He gas. The results can be good references to measurement of other plasmas operated at atmospheric pressure introduced in following subsections. Two electrodes for anode and cathode had a 2-mm bore and a 4-mm hole length, and these electrodes were separated by a 1.5-mm thick ceramic disk also having the 2-mm bore. Two of ZnSe windows were equipped to seal the discharge region and transmit the CO_2 laser beam. Gas pressure inside the small chamber was controlled in a range from several tens to hundreds Torr.
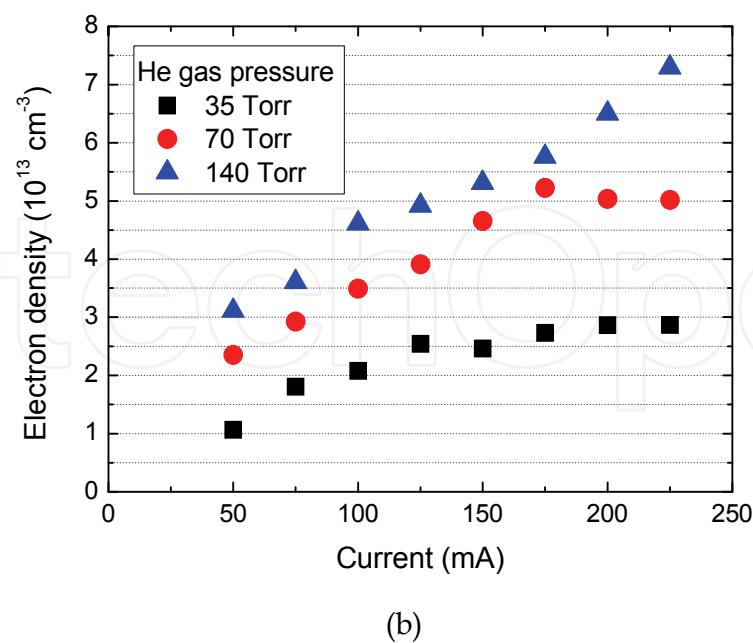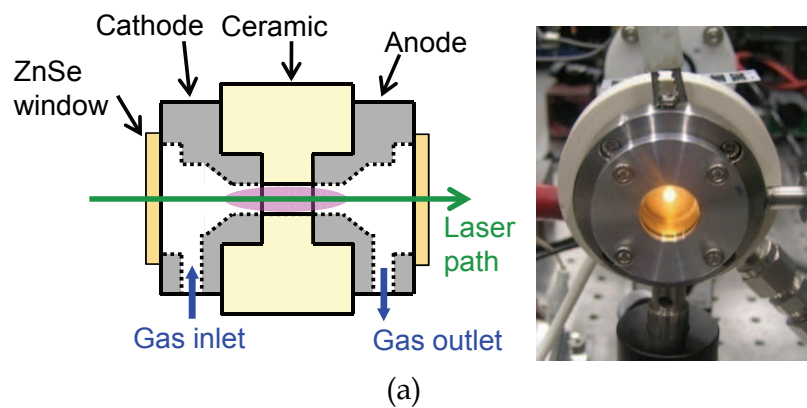

(a)

(b)

Fig. 5. (a) Cross-sectional diagram and photograph of short hollow cathode (HC) discharge. (b) Dependence of electron density on discharge current in the short HC discharge in He gas at three values of gas pressure.

Figure 5(b) shows dependences of electron density in the short HC discharge on the discharge current measured at several He gas pressures. In the calculation of electron density from the phase shift signal, we used two assumptions that the plasma was uniform along the CO_2 laser path and its effective length was 9.5 mm. The electron density in the discharge increased monotonically with the increase of the discharge current and the gas pressure. This result indicates that the CO_2-laser heterodyne interferometer is able to measure appropriate dependence of electron density on the gas pressure, because the electron density inside the high-pressure plasma must be increased at higher pressure by the slower drift velocity of electrons due to frequent collisions with gas particles when the discharge current is the same as that at lower pressure.

Here, the minimum sensitivity of electron density in our CO_2-laser heterodyne interferometer is introduced. The minimum electron density which we recorded in the short HC discharge was corresponds to a line integrated electron density $n_e d$ of 7×10^{12} cm^{-2} with a detected phase shift around 0.1 degree (Choi et al., 2009). However, the signal to noise ratio, for instance shown in Fig. 3, showed that the minimum sensitivity should be at least six times better than that. Therefore, it could be estimated that the minimum detectable phase shift in our system was about 0.02 degree, corresponding to $n_e d$ of 1×10^{12} cm^{-2}, which is much smaller than the minimum sensitivity of Stark broadening measurement (Laux et al, 2003).

3.2 Atmospheric-pressure DC discharge in open space

Figure 6(a) shows a schematic diagram of DC discharge in open space operated in a He gas flow ejected from a tubular cathode to a pin anode. The cylindrical tubular cathode, whose outer and inner diameters were 3.1 and 2.1 mm, and the pin anode with a 0.5-mm diameter were faced to the cathode with a 3-mm gap. The measurement point between the cathode and the anode was scanned by putting the whole discharge device on a three-dimensional mechanical movement stage. The influence of temporal evolutions of the gas-particle density on the measured phase shift can be seen in Fig. 6(b) showing the phase-shift signals observed in the atmospheric-pressure DC discharge using two different flow rates of He gas (1 and 2 L/min). This measurement result clearly suggests that the contribution of the Joule heating on temporal evolution of the phase shift becomes much greater in the discharge operated at atmospheric pressure and the gas-particle component in the phase shift, $\Delta \Phi_g$, has large dependence on the gas flow velocity. The fast time constant and large amplitude of $\Delta \Phi_g$ in both rising and falling periods of applied voltage in lower gas flow rate was due to less cooling effect by neutral gas particles.

In order to obtain radial distributions of electron density in the high-pressure plasmas, which cannot be evaluated by photographic observations, spatial distributions of line-integrated electron density and inverse Abel transformation of the distributions are required. This diagnostic method of radial distribution is also applied for excited species measurements in the high-pressure plasmas by a laser absorption spectroscopy (LAS) and a laser induced fluorescence (LIF) methods (Urabe et al., 2010). Figure 7(a) shows two spatial distributions of the line-integrated electron density, $\int n_e dl(x)$, measured near the tubular cathode and the pin anode in the DC discharge scanning the laser beam perpendicularly to the gas-flow axis. Using the CO_2-laser heterodyne interferometer with appropriate control of

the beam radius around the tested plasma source, the spatial distribution of electron density with enough quality for the inverse Abel transformation can be measured.
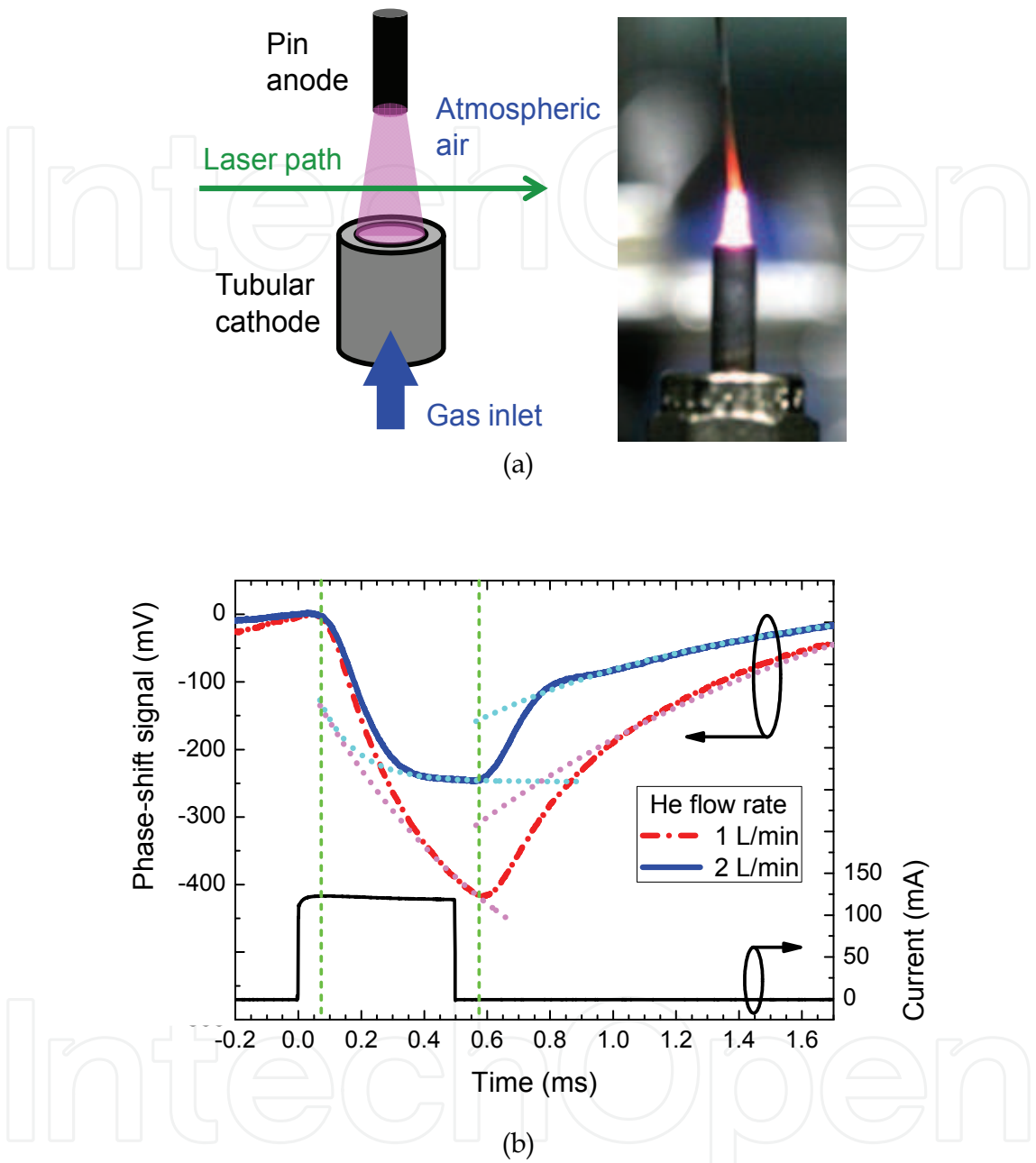

(a)

(b)

Fig. 6. (a) Schematic diagram and photograph of atmospheric-pressure DC discharge in open space. (b) Temporal evolutions of phase-shift signal in the DC discharge measured changing He gas flow rate.

Calculation results of the inverse Abel transformation corresponding to the radial distribution of electron density, $n_e(r)$, at the measurement points in the DC discharge are shown in Fig. 7(b). The calculated radial distributions showed two different structures which were a hollow shape near the cathode and a center-peaked shape near the anode, having a good agreement with the electrode structures. The inverse Abel transformation was performed using a following equation (Lochte-Holtgreven, 1968),

$$n_e(r) = -\frac{1}{\pi} \int_r^\infty \frac{d}{dx}\left(\int n_e \, dl(x)\right) \frac{dx}{\sqrt{x^2 - r^2}} \; . \tag{7}$$
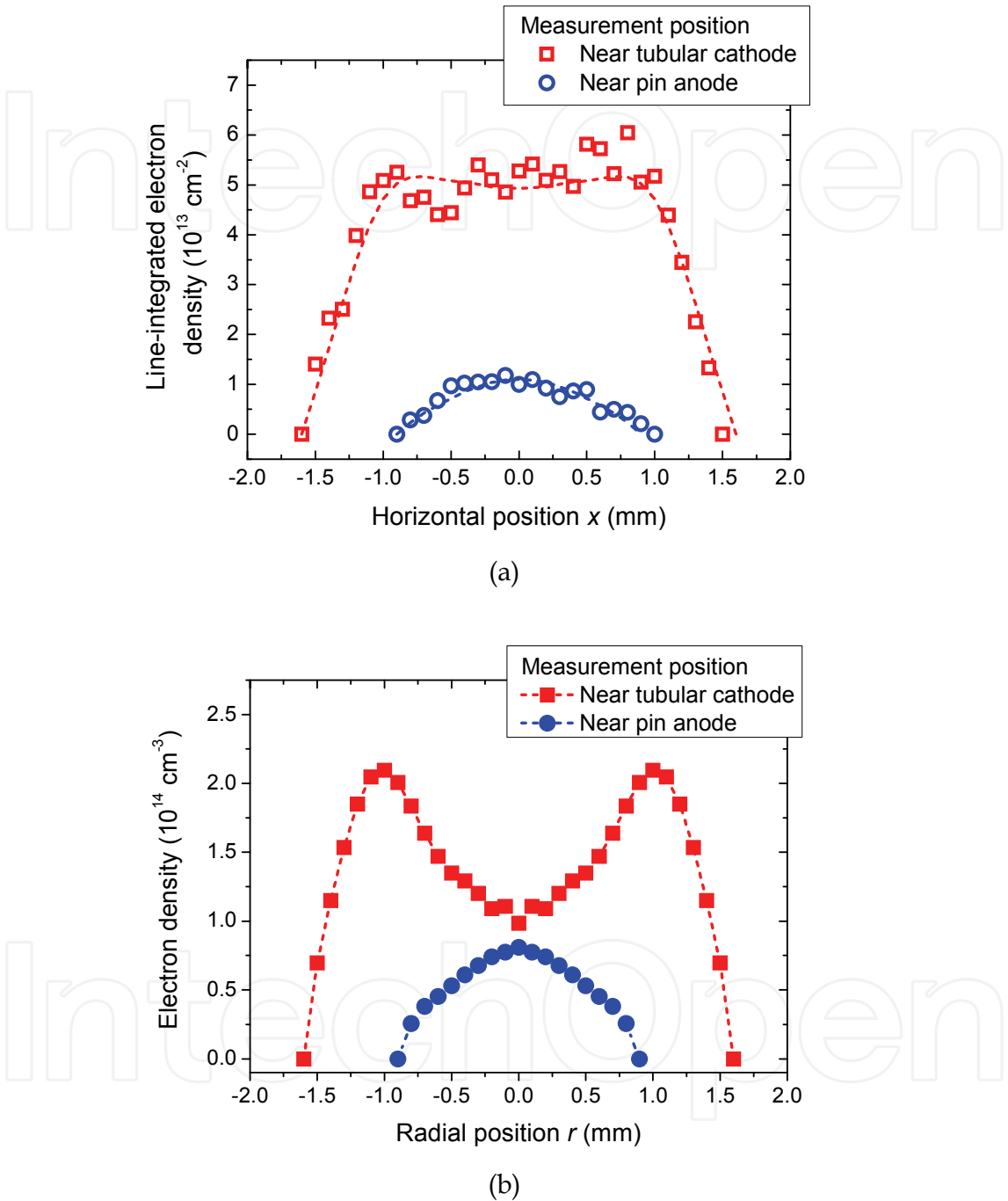

(a)

(b)

Fig. 7. (a) Spatial distributions of line-integrated electron density measured in DC plasma jet near tubular cathode and pin anode. (b) Radial distributions of electron density derived from line-integrated electron density using inverse Abel transformation (Choi et al., 2009).

The calculated results in Fig. 7(b) indicate that total amounts of the electrons near the cathode and the anode are significantly different in this DC discharge and there must be another kind of negatively charged particles delivering the discharge current and keeping

its continuity. Considering that electron density near the central axis of the gas flow was not different at both measurement points, there were some losing mechanisms of the electrons outside of the He gas flow where ambient air contaminates into the flow. The electron loss was mainly due to an electron attachment process with O_2 molecules presenting in the ambient air in the DC discharge, because of µm-order short diffusion lengths of electrons in the atmospheric-pressure gas conditions which could be derived from calculations of electron diffusion coefficient (Hargelaar & Pitchford, 2005) and measurement results of electron lifetime (Moselhy et al., 2003). Whereas this negative-ion density, for example O_2^- ions, cannot be detected by the CO_2-laser heterodyne interferometer, this selectivity of negatively charged particles in the interferometer enables us to distinguish kinds and fractions of the negatively charged particle inside the high-pressure plasmas with the estimation of total amount of the charged particles from the discharge current amplitude.

3.3 Pulsed AC discharge at atmospheric pressure

For the measurement of electron density inside the high-pressure plasmas driven by kHz-order AC applied voltage, the temporal resolution of CO_2-laser heterodyne interferometer using the lock-in amplifier is often insufficient for direct measurement of temporal evolutions of electron density. In order to depict spatiotemporal structures of electron density inside such plasma sources, for example dielectric barrier discharges (DBDs) (Kogelschatz, 2003; Becker et al., 2005) and ns-order short pulsed discharges (Namihira et al., 2003; Walsh & Kong, 2007), it has been confirmed that an amplitude modulation of the kHz-order applied voltage at a frequency of a few hundreds Hz and additional measurement of a millimeter-wave (mm-wave) transmission method are effective.

Figure 8(a) shows a schematic diagram of atmospheric-pressure glow discharge (APGD) tested in our group. The APGD is a major kind of DBDs generating homogeneous plasmas with atmospheric-pressure He gas and kHz-order AC applied voltage (Kanazawa et al., 1988). Powered (upper side) and grounded (lower side) stainless-steel electrodes were round, and their diameters were 60 mm. Dielectric barriers of 1-mm thick alumina were placed on the electrodes' surface and a gap distance between the two barriers was set at 6.0 mm. Whole electrode setup was installed in a vacuum chamber with a pair of ZnSe windows to control the gas compositions and pressures. In the measurement of APGD, we used a pair of ZnSe lens with longer focal length (20 cm), in order to get constant beam shape in whole discharge region with 60-mm length along the CO_2 laser path. Therefore, the spatial resolution of the interferometer was worse than the measurement of small-scale DC plasmas explained in above subsections.

To divide the phase-shift signal into two components of the electron and gas-particle densities in a similar way to that used for the small-scale DC discharges, we used a square-pulse amplitude modulation at 125 Hz for the 30-kHz AC applied voltage, whose modulation-signal waveform is shown in Fig. 8(b). Using this amplitude modulation, the temporal evolution of phase shift has the fall and rise slopes in the both ends of modulation signal similar to that in the measurement of pulsed DC discharges. However, in the measurement of AC discharge, the phase-shift signal at the start-up timing of applied voltage (around −3.5 ms in the abscissa axis of Fig. 8(b)) is unsuitable for the derivation of the electron-density component in the phase shift. At this timing, the signal associated with the electron density was smoothed by the step-wise increase due to intermittent discharges

in the APGD, and the influence of this smoothing effect on the phase-shift signal could not be resolved. Therefore, the measured phase-shift waveform should be divided into two components only at the cut-off timing of applied voltage (around 0 ms in Fig. 8(b)). Calculation procedure of the temporally-averaged electron density after dividing the two components is the same as the calculation in DC discharges.
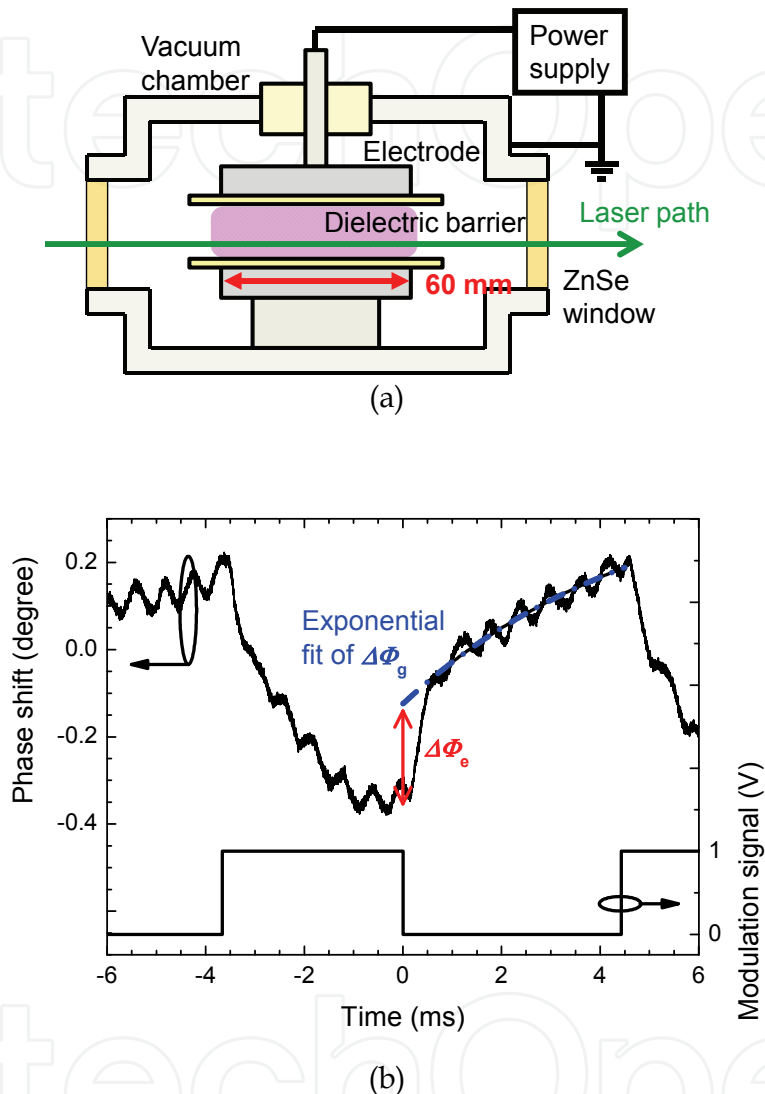

(a)

(b)

Fig. 8. (a) Cross-sectional diagram of parallel-plate dielectric barrier discharge (DBD). (b) Example temporal evolution of phase shift by the parallel-plate DBD together with amplitude modulation signal of 30-kHz AC applied voltage (Urabe et al., 2011).

The spatial distribution of the electron-density component in the phase shift and the calculated temporally-averaged electron density from the four signal waveforms measured under the same condition are shown in Fig. 9. The points and both ends of error bars indicate the averaged value and the maximum and minimum values in each measurement. The electron-density distribution inside the APGD was localized near the dielectric barriers, and this result had a good agreement with reported results of computational simulations in similar geometries (Massines et al., 1998, 2003; Martens et al., 2009). The electron density near the powered electrode was approximately two times larger than that near the

grounded electrode in each gas composition. This asymmetric distribution was probably caused by diffusion of the discharge current flow into the chamber wall from the powered electrode not flowing into the grounded electrode.

To get temporally resolved information of the electron density inside the APGD, we inserted a mm-wave at 55 GHz through the vacuum chamber and measured temporal evolutions of the transmitted mm-wave intensity using a pair of horn antennas. In this mm-wave transmission method, spatial distributions of electron density cannot be measured because of the diffraction limit of the mm-wave. Details of the experimental setup and the calculation procedure of spatially-averaged electron density are introduced in our previous paper (Urabe et al., 2011). The temporal evolution of spatially-averaged electron density in the APGD derived from absorption ratio of the mm-wave in the plasma is shown in Fig. 10,
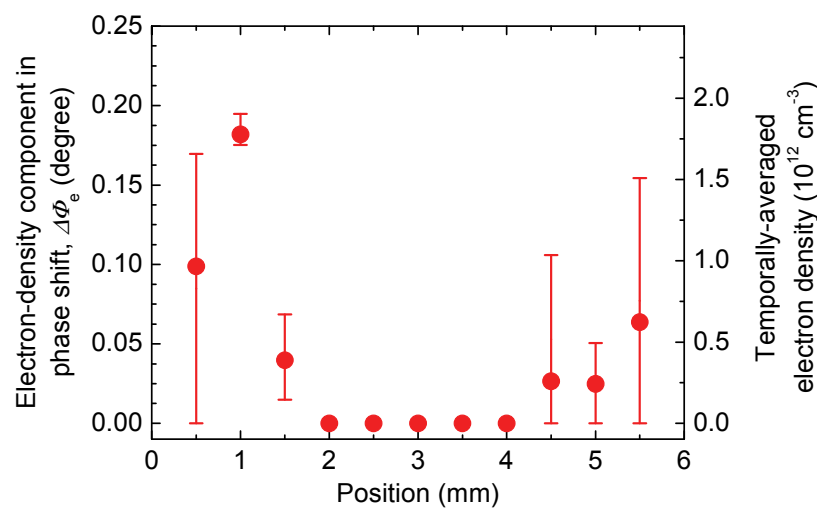
Fig. 9. Spatial distribution of electron-density component in phase shift and calculated temporally-averaged electron density in APGD (Urabe et al., 2011).
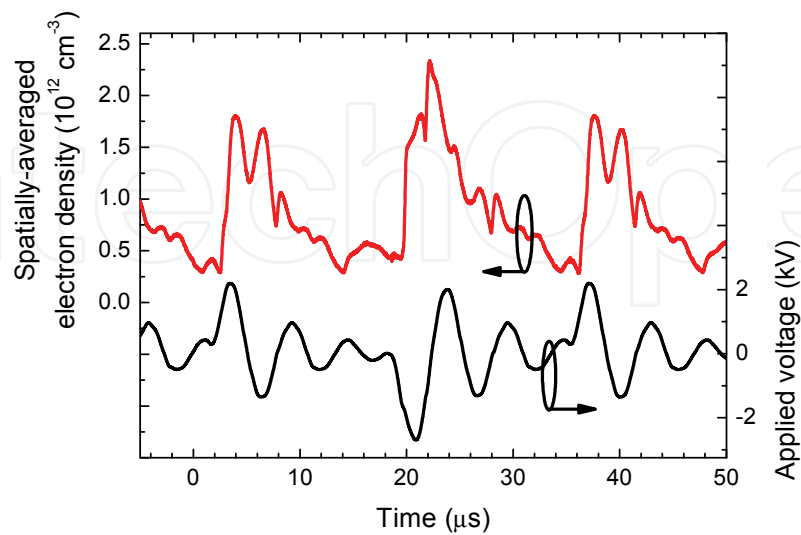

Fig. 10. Temporal evolution of spatially-averaged electron density in APGD measured by mm-wave transmission method under same conditions as interferometer measurement (Fig. 9), together with applied-voltage waveform (Urabe et al., 2011).

together with the waveform of applied voltage. The electron density increased after the positive- and negative-main pulses around 2.6 and 19.0 μs in the abscissa time axis, and there were small increases in electron density after the main pulses caused by weak discharges in the ringing part of applied voltage.

From the measurement results of the CO_2-laser heterodyne interferometer and the mm-wave transmission method applied to the same plasma source, spatial distribution of temporal-peak electron density can be calculated dividing the temporally-averaged electron densities by a duty ratio of plasma. The duty ratio of plasma is the ratio of temporally-averaged electron density to temporal-peak density in the result of the mm-wave transmission measurement, and it indicates the temporally averaging effects of the CO_2-laser heterodyne interferometer. In an example case of the APGD measurement shown in Figs. 9 and 10, the calculated duty ratio of plasma was 0.33. Then, the temporal-peak electron densities near the dielectric barriers were derived approximately 5×10^{12} cm^{-3} on the side of the powered electrode and 2×10^{12} cm^{-3} on the grounded electrode.

4. Concluding remarks

In this chapter, we reviewed experimental studies for electron-density measurement in small-scale plasmas operated at high and atmospheric pressures using the CO_2-laser heterodyne interferometer, from brief theoretical introduction of the interferometer to specific measurement results in the high-pressure plasma sources. It should be noted that separation of the CO_2 laser beam's phase shift into two components, which are due to changes of electron and gas-particle densities, is the most important procedure for the measurement in high-pressure plasmas, and pulse modulation of applied voltage is indispensable for the separation at the rise and fall timings of the modulation signal.

From the experimental results of the interferometer in high-pressure plasmas driven by pulsed DC voltage, fundamental properties of our interferometer including the minimum sensitivity of line-integrated electron density and the spatial resolution could be evaluated. Because these properties are changed due to specifications of the laser source and the phase detecting system, they must be confirmed in each setup of the interferometer before practical measurements. In addition to the interferometer, a mm-wave transmission method with a good temporal resolution was used to AC-voltage driven plasmas having ns-order fast temporal behavior. This novel combination method has potentials to be applied to the refractive-index measurements requiring both spatial and temporal high resolutions.

5. Acknowledgments

6. References

Acedo, P.; Lamela, H.; Sanchez, M.; Estrada, T. & Sanchez, J. (2004). CO$_2$ (λ_m=10.6µm) He-Ne (λ_c=633nm) two-color laser interferometry for low and medium electron density measurements in the TJ-II Stellarator. *Review of Scientific Instruments,* Vol. 75, pp. 4671-4677

Adler, F. & Kindel, E. (2003). Absolute Determination of Electron Densities in a Micro Hollow Cathode Discharge by Dual Wavelength Interferometry. *Proceedings of XXVIth International Conference on Phenomena in Ionized Gases,* Greifswald, Germany, July 15-20, 2003

Allen, C.W. (1973). *Astrophysical Quantities,* The Athlon Press, London, UK

Babayan, S.E.; Jeong, J.Y.; Tu, V.J.; Park, J.; Selwyn, G.S. & Hicks, R. F. (1998). Deposition of silicon dioxide films with an atmospheric-pressure plasma jet. *Plasma Sources Science and Technology,* Vol. 7, pp. 286-288

Becker, K.H.; Kogelschatz, U.; Schoenbach, K.H. & Barker, R.J. (Eds.). (2005). *Non-Equilibrium Air Plasmas at Atmospheric Pressure,* Institute of Physics, Bristol, UK

Bruggeman, P. & Leys, C. (2009). Non-thermal plasmas in and in contact with liquids. *Journal of Physics D: Applied Physics,* Vol. 42, pp. 053001-1-28

Chang, J.S. (1973). The inadequate reference electrode, a widespread source of error in plasma probe measurements. *Journal of Physics D: Applied Physics,* Vol. 6, pp. 1674-1683

Chang, J.S. & Laframboise, J.G. (1976). Probe theory for arbitrary shape in a large Debye length, stationary plasma. *Physics of Fluids,* Vol. 19, pp. 25-31

Choi, J.Y.; Takano, N.; Urabe, K. & Tachibana, K. (2009). Measurement of electron density in atmospheric pressure small-scale plasmas using CO$_2$-laser heterodyne interferometry. *Plasma Sources Science and Technology,* Vol. 18, pp. 035013-1-8

Hagelaar, G.J.M. & Pitchford, L.C. (2005). Solving the Boltzmann equation to obtain electron transport coefficients and rate coefficients for fluid models. *Plasma Sources Science and Technology,* Vol. 14, pp. 722-733

Hutchinson, I.H. (2002). *Principles of Plasma Diagnostics,* Cambridge University Press, Cambridge, UK

Ichiki, T.; Taura, R. & Horiike, Y. (2004). Localized and ultrahigh-rate etching of silicon wafers using atmospheric-pressure microplasma jets. *Journal of Applied Physics,* Vol. 95, pp. 35-39

Ito, Y.; Sakai, O. & Tachibana, K. (2010). Measurement of electron density in a microdischarge-integrated device operated in nitrogen at atmospheric pressure using a millimetre-wave transmission method. *Plasma Sources Science and Technology,* Vol. 19, pp. 025006-1-9

Kanazawa, S.; Kogoma, M.; Moriwaki, T.; & Okazaki, S. (1988). Stable glow plasma at atmospheric pressure. *Journal of Physics D: Applied Physics,* Vol. 21, pp. 838-840

Kogelschatz, U. (2003). Dielectric-barrier Discharges: Their History, Discharge Physics, and Industrial Applications. *Plasma Chemistry and Plasma Processing,* Vol. 23, pp. 1-46

Kong, M.G.; Kroesen, G.; Morfill, G.; Nosenko, T.; Shimizu, T.; van Dijk, J. & Zimmermann, J.L. (2009). Plasma medicine: an introductory review. *New Journal of Physics,* Vol. 11, pp. 115012-1-35

Kono, A. & Iwamoto, K. (2004). High-Spatial-Resolution Multichannel Thomson Scattering Measurements for Atmospheric Pressure Microdischarge. *Japanese Journal of Applied Physics,* Vol. 43, pp. L1010-L1013

Laux, C.O.; Spence, T.G.; Kruger, C.H. & Zare, R.N. (2003). Optical diagnostics of atmospheric pressure air plasmas. *Plasma Sources Science and Technology,* Vol. 12, pp. 125-138

Leipold, F.; Stark, R.H.; El-Habachi, A. & Schoenbach, K.H. (2000). Electron density measurements in an atmospheric pressure air plasma by means of infrared heterodyne interferometry. *Journal of Physics D: Applied Physics,* Vol. 33, pp. 2268-2273

Lochte-Holtgreven, W. (Ed.). (1968). *Plasma Diagnostics,* North-Holland Publishing, Amsterdam, Netherlands

Martens, T.; Brok, W.J.M.; van Dijk, J. & Bogaerts, A. (2009). On the regime transitions during the formation of an atmospheric pressure dielectric barrier glow discharge. *Journal of Physics D: Applied Physics,* Vol. 42, pp. 122002-1-5

Massines, F.; Rabehi, A.; Decomps, P.; Gadri, R.B.; Segur, P. & Mayoux, C. (1998). Experimental and theoretical study of a glow discharge at atmospheric pressure controlled by dielectric barrier. *Journal of Applied Physics,* Vol. 83, pp. 2950-2957

Massines, F.; Segur, P.; Gherardi, N.; Khamphan, C. & Ricard, A. (2003). Physics and chemistry in a glow dielectric barrier discharge at atmospheric pressure: diagnostics and modeling. *Surface and Coatings Technology,* Vol. 174–175, pp. 8-14

Moselhy, M.; Petzenhauser, I.; Frank, K. & Schoenbach, K.H. (2003). Excimer emission from microhollow cathode argon discharges. *Journal of Physics D: Applied Physics,* Vol. 36, pp. 2922-2927

Namihira, T.; Wang, D.; Katsuki, S.; Hackam, R. & Akiyama, H. (2003). Propagation Velocity of Pulsed Streamer Discharges in Atmospheric Air. *IEEE Transactions on Plasma Science,* Vol. 31, pp. 1091-1094

Nozaki, T.; Sasaki, K.; Ogino, T.; Asahi, D. & Okazaki, K. (2007). Microplasma synthesis of tunable photoluminescent silicon nanocrystals. *Nanotechnology,* Vol. 18, pp. 235603-1-6

Paschen, F. (1889). Ueber die zum Funkenübergang in Luft, Wasserstoff und Kohlensäure bei verschiedenen Drucken erforderliche Potentialdifferenz. *Annalen der Physik,* Vol. 273, pp. 69–96

Sakai, O.; Sakaguchi, T.; Ito, Y. & Tachibana, K. (2005). Interaction and control of millimetre-waves with microplasma arrays. *Plasma Physics and Controlled Fusion,* Vol. 47, pp. B617-B627

Tachibana, K.; Kishimoto, Y. & Sakai, O. (2005(a)). Measurement of metastable He*(23S1) density in dielectric barrier discharges with two different configurations operating at around atmospheric pressure. *Journal of Applied Physics,* Vol. 97, pp. 123301-1-7

Tachibana, K.; Kishimoto, Y.; Kawai, S.; Sakaguchi, T. & Sakai, O. (2005(b)). Diagnostics of microdischarge-integrated plasma sources for display and materials processing. *Plasma Physics and Controlled Fusion,* Vol. 47, pp. A167-A177

Urabe, K.; Morita, T.; Tachibana, K. & Ganguly, B.N. (2010). Investigation of discharge mechanisms in helium plasma jet at atmospheric pressure by laser spectroscopic measurements. *Journal of Physics D: Applied Physics,* Vol. 43, pp. 095201-1-13

Urabe, K.; Sakai, O. & Tachibana, K. (2011). Combined spectroscopic methods for electron-density diagnostics inside atmospheric-pressure glow discharge using He/N2 gas mixture. *Journal of Physics D: Applied Physics,* Vol. 44, pp. 115203-1-11

von Engel, A. (1994). *Ionized Gases,* American Institute of Physics, New York, USA

Walsh, J.L. & Kong, M.G. (2007). 10 ns pulsed atmospheric air plasma for uniform treatment of polymeric surfaces. *Applied Physics Letters,* Vol. 91, pp. 241504-1-3

Yariv, A. (1997). *Optical Electronics in Modern Communications,* Oxford University Press, New York, USA
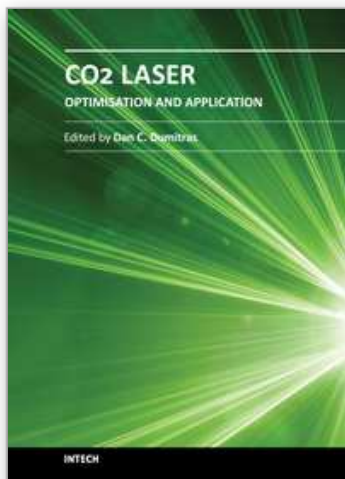
CO2 Laser - Optimisation and Application

Edited by Dr. Dan C. Dumitras

The present book includes several contributions aiming a deeper understanding of the basic processes in the operation of CO2 lasers (lasing on non-traditional bands, frequency stabilization, photoacoustic spectroscopy) and achievement of new systems (CO2 lasers generating ultrashort pulses or high average power, lasers based on diffusion cooled V-fold geometry, transmission of IR radiation through hollow core microstructured fibers). The second part of the book is dedicated to applications in material processing (heat treatment, welding, synthesis of new materials, micro fluidics) and in medicine (clinical applications, dentistry, non-ablative therapy, acceleration of protons for cancer treatment).

How to reference

In order to correctly reference this scholarly work, feel free to copy and paste the following:

Keiichiro Urabe and Kunihide Tachibana (2012). Heterodyne Interferometer for Measurement of Electron Density in High-Pressure Plasmas, CO2 Laser - Optimisation and Application, Dr. Dan C. Dumitras (Ed.), ISBN: 978-953-51-0351-6, InTech, Available from: http://www.intechopen.com/books/co2-laser-optimisation-and-application/heterodyne-interferometer-for-measurement-of-electron-density-in-high-pressure-plasmas

INTECH
open science | open minds